

# Measurement of the $e^+e^- \rightarrow ZZ$ Production Cross Section

C. Loomis

*European Laboratory for Particle Physics (CERN), CH-1211 Geneva 23, Switzerland*

for the ALEPH Collaboration

The  $e^+e^- \rightarrow ZZ$  cross sections at  $\sqrt{s} = 182.7$  and  $188.6$  GeV have been measured using the ALEPH detector and the 1997 and 1998 LEP2 data samples representing integrated luminosities of  $56.8$  and  $173.5 \text{ pb}^{-1}$ , respectively. The selections cover all of the visible  $ZZ$  final states and yield cross section measurements of

$$\sigma_{\mathcal{N}C2}(182.7 \text{ GeV}) = 0.22 \pm 0.18_{0.22} \text{ (stat.)} \pm 0.04 \text{ (syst.) pb, and}$$

$$\sigma_{\mathcal{N}C2}(188.6 \text{ GeV}) = 0.63 \pm 0.12 \text{ (stat.)} \pm 0.05 \text{ (syst.) pb,}$$

consistent with the Standard Model values of  $0.25$  and  $0.63$  pb, respectively.

## I. INTRODUCTION

The successful operation of LEP at and above the  $ZZ$  threshold in 1997 and 1998 allows, for the first time, a sizeable number of pair-produced resonant  $Z$  bosons to be observed and consequently, the production cross section of  $e^+e^- \rightarrow ZZ$  to be measured. This note principally describes the  $188.6$  GeV measurement but also uses this analysis to measure the cross section at  $182.7$  GeV.

Within the Standard Model, the process  $e^+e^- \rightarrow ZZ$  proceeds dominantly via the two “ $\mathcal{N}C2$ ” diagrams which involve the  $t$ -channel exchange of an electron. For a center-of-mass energy of  $188.6$  ( $182.7$ ) GeV, the total  $\mathcal{N}C2$  cross section is  $0.63$  ( $0.25$ ) pb [1]. Other contributions to the  $ZZ$  cross section for “off-shell” production are small and are treated here as an additional background. The measurement of the  $\mathcal{N}C2$  cross section for  $ZZ$  production is analogous to the measurement of the  $CC03$  cross section for  $WW$  production.

A total integrated luminosity of  $173.5 \pm 1.7 \text{ pb}^{-1}$  at  $\sqrt{s} = 188.6$  GeV in 1998 and  $56.8 \pm 0.6 \text{ pb}^{-1}$  at  $\sqrt{s} = 182.7$  GeV in 1997 was collected.

## II. EVENT SELECTION

The following analyses are sensitive to all visible final states arising from  $ZZ$  production. With one exception, the event selections follow closely those used for the Higgs boson searches [2]. A dedicated analysis was developed for the  $\ell\nu\bar{\nu}$  final state.

Two parallel analyses (with significant overlap) measure the  $ZZ$  production cross section. The first is an entirely cut-based analysis which uses the  $q\bar{q}q\bar{q}$ ,  $q\bar{q}\nu\bar{\nu}$ ,  $\ell\ell XX$ , and  $\ell^+\ell^-\nu\bar{\nu}$  channels. (The symbol  $\ell$  denotes electrons and muons and  $X$  denotes quarks and leptons throughout this note.) The second analysis (generically called the “NN” analysis) replaces the cut-based selections in the  $q\bar{q}q\bar{q}$  and  $q\bar{q}\nu\bar{\nu}$  channels with neutral networks and introduces an additional neural network to identify the  $\tau\tau q\bar{q}$  final state. Use of shapes of the neural network outputs further improves the expected resolution of the second analysis.

### A. $ZZ \rightarrow \ell\ell XX$ Final States

The  $\ell\ell XX$  selection is based upon the  $h\ell^+\ell^-$  search [2]. To retain efficiency for  $\ell\ell\ell\ell$  final states, the missing energy requirement for four-prong events is removed. The lepton pair with the mass closest to  $m_Z$  is used as the mass of the first  $Z$  candidate (Fig. 1); that of the second candidate is the mass recoiling against the two leptons. To improve the resolution, the lepton mass is constrained to  $m_Z$  in the calculation of the recoil mass.

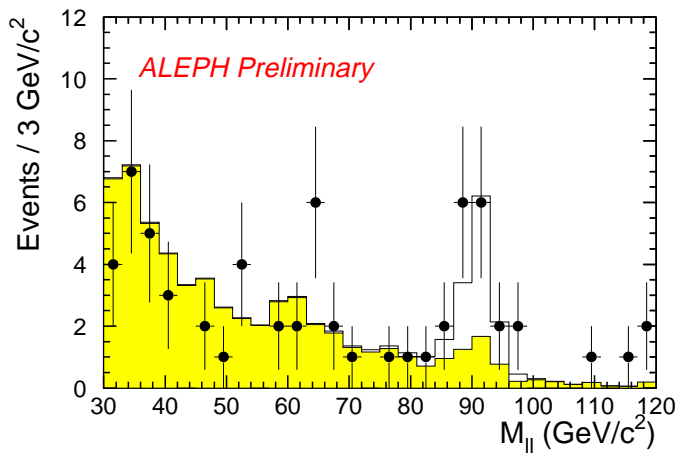


FIG. 1. The distribution of masses for the  $\ell\ell XX$  channel. All cuts have been applied except the elliptical mass cut. The grey histogram shows the expected background and the hollow histogram, the expected signal.

To further reduce background levels, cuts are placed on the invariant mass of the two leptons and the recoil mass. As the leptonic invariant mass and recoil mass have different resolutions, an elliptical cut is defined using

$$r^2 = \left( \frac{m_{\ell\ell} - m_Z}{\sigma_{m_{\ell\ell}}} \right)^2 + \left( \frac{m_{\text{recoil}} - m_Z}{\sigma_{m_{\text{recoil}}}} \right)^2$$

where  $\sigma_{m_{\ell\ell}} = 2.5$  and  $\sigma_{m_{\text{recoil}}} = 3.3 \text{ GeV}/c^2$  are the approximate resolutions.

The performance of this selection is summarized in Table I. Figure 1 shows the invariant mass of the two leptons in the  $\ell\ell XX$  analysis with the elliptical mass cut removed.

Systematic uncertainties from lepton identification, tracking resolutions, and event kinematics have been studied. The dominant systematic uncertainty for the signal is the uncertainty arising from the momentum resolution of the leptons, leading to a total relative uncertainty on the selection efficiency of 1.5%. The relative uncertainty on the expected number of background events is 30% (0.34 events), dominated by limited Monte Carlo statistics.

### B. Hadronic Final States— $ZZ \rightarrow q\bar{q}q\bar{q}$ (CUT Analysis)

The  $ZZ \rightarrow q\bar{q}q\bar{q}$  final state has the largest branching fraction, but also the largest background. Although not the main thrust, this selection has a significant efficiency for the  $\tau\tau q\bar{q}$  final state. Including the  $ZZ \rightarrow q\bar{q}\tau\tau$  final state, this selection covers 54% of the total cross section. This analysis is similar to the four-quark selection in the Higgs boson search [2].

After the preselection, a cut to reduce the overlap between the  $q\bar{q}q\bar{q}$  and the  $q\bar{q}\mu^+\mu^-$  selection is applied. (Standard ISR cuts remove the  $q\bar{q}e^+e^-$  events.) Accepted events have an invariant mass of the two most energetic muon candidates ( $m_{\mu\mu}$ ) less than  $50 \text{ GeV}/c^2$  and satisfy the condition  $p_1 + p_2 - m_{\mu\mu} < 35 \text{ GeV}/c$ , where  $p_1$  and  $p_2$  are the momenta of the two muons. For events with only one identified muon, this cut reduces to  $p_1 < 35 \text{ GeV}/c$ . This cut negligibly affects the efficiency for the  $q\bar{q}q\bar{q}$  final state but rejects more than 97% of the overlap with the  $q\bar{q}\mu^+\mu^-$  channel. This cut also rejects a small fraction of the WW background.

Further improvements to the selection rely on the b-tagging and dijet mass information. The dijet masses are calculated after applying a four-constraint fit to the jet four-momenta, imposing energy-momentum conservation as in Ref. [3]. A four variable neural network produces a value for each jet,  $\eta_i$ , which is near unity for b-jets and near zero for other jets.

The four-jet analysis is split into three sub-analyses—a  $b\bar{b}b\bar{b}$  selection, a  $b\bar{b}q\bar{q}$  selection, and a non-b-quark selection. For the cross section measurement, the two b-selections are treated as a single channel. The first two use b-tagging

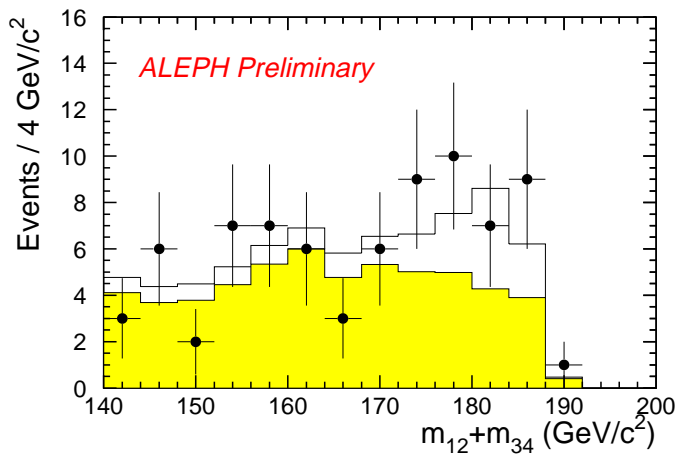


FIG. 2. The distribution of masses for the  $q\bar{q}q\bar{q}$  channel with b-tagging. All cuts have been applied except the elliptical mass cut. The hollow histogram is the contribution from the signal and the darker region that from the background.

cuts to reduce the backgrounds. The last replaces the b-tagging cuts with strict mass requirements to retain efficiency for the majority of ZZ events ( $\sim 62\%$ ) which do not contain b-quark jets.

The  $b\bar{b}b\bar{b}$  cuts select events with high b-content, well-isolated jets, and large dijet masses according. The selection aimed at the  $b\bar{b}q\bar{q}$  final state introduces tight mass requirements. The quantities  $\chi_W$  and  $\chi_Z$  defined as

$$\chi_i^2 = \left( \frac{m_{12} + m_{34} - 2m_i}{\sigma_S^i} \right)^2 + \left( \frac{m_{12} - m_{34}}{\sigma_D^i} \right)^2$$

where  $i$  stands for W or Z contain the mass information. The contours of constant  $\chi_W$  and  $\chi_Z$  define two ellipses referred to as WW and ZZ ellipses throughout this section. The quantities  $\sigma_S^i$  and  $\sigma_D^i$  are approximately the resolutions of the sum and the difference of the dijets masses for the correct dijet combination, respectively. The values used for  $\sigma_S^i$  are, respectively, 3 and 4  $\text{GeV}/c^2$  for the ZZ and the WW ellipse and 16 and 10  $\text{GeV}/c^2$  for  $\sigma_D^i$ . The  $b\bar{b}q\bar{q}$  selection requires that at least one jet combination falls inside the ZZ ellipse with  $\chi_Z < 2.40$ . The dijet not containing the most poorly b-tagged jet must be compatible with  $Z \rightarrow b\bar{b}$  in terms of the b-tagging.

The selection for  $q\bar{q}q\bar{q}$  events without b-jets further tightens the ZZ ellipse to  $\chi_Z < 1.75$  and reduces the WW background by requiring that no dijet combination falls inside a WW ellipse with  $\chi_W < 1.60$ . To maintain the statistical independence of the b and non-b selections, this selection accepts only those events which have not been previously selected by the  $b\bar{b}b\bar{b}$  or  $b\bar{b}q\bar{q}$  cuts.

The performance of this selection is summarized in Table I. Figure 2 shows the sum of the dijet masses for the  $b\bar{b}b\bar{b}$  and  $b\bar{b}q\bar{q}$  selections with the elliptical mass cut removed.

The systematic uncertainties in this channel include uncertainties from the modeling of b-physics, tracking discrepancies, cross section uncertainties, gluon splitting, Z branching fractions, and jet corrections. The total relative systematic uncertainties on the signal efficiencies are 3% and 2% for the b and non-b selections respectively. The relative uncertainties for the background are 22% and 7%.

### C. $q\bar{q}q\bar{q}$ Neural Network Selection

Events are forced into four jets, and as in the Higgs boson search [2], a multi-layer neural network is trained to reject background events. For the ZZ selection, 6 new variables add discriminating power to the 17 variables used in the Higgs boson search. The additional variables are 1)  $m_{34}$ , the dijet invariant mass, 2) the missing energy in the event, 3)  $\max(\max(E_{\text{charged track}})/E_{\text{jet}})$ , the maximum scaled energy among all jets of the most energetic charged track in a jet, 4)  $(m_{12} - m_{34})^2 + (m_{34} - m_Z)^2$ , 5) the thrust of the event, and 6) the sphericity of the event. The reconstructed Z masses,  $m_{12}$  and  $m_{34}$ , are calculated from the dijet combination with the largest neural network output.

This analysis has a 31.5% signal efficiency for  $q\bar{q}q\bar{q}$ . It expects 16.9 ZZ signal events and 19.7 background events. The background expectation includes a correction for gluon splitting to heavy quarks, which is not correctly simulated. This analysis selects 31 events.

The preliminary study of systematic uncertainties follows the prescription used for the Higgs boson search. Uncertainties in the event selection are studied by reweighting the neural network inputs and recalculating the signal efficiency and number of expected background events. All of the inputs were reweighted, including inputs relating to b-tagging. In addition,  $\alpha_s$  was varied within its experimental uncertainty. The total relative uncertainty on the ZZ signal efficiency is 3.1%. The relative uncertainty on the background is 13.7% (2.70 events).

With this selection, the expected statistical uncertainty on the measured cross section is 36%. The expected uncertainty is reduced further by using the neural net output distribution to subdivide the analysis into six pieces. Because pieces with higher neural net outputs are more pure than pieces with low neural net outputs, combining the six analysis pieces results in the lower expected uncertainty of 33%.

#### D. $q\bar{q}\nu\bar{\nu}$ Channel (CUT Analysis)

Approximately 30% of the ZZ events have a  $q\bar{q}\nu\bar{\nu}$  topology, characterized by missing and visible masses consistent with the Z mass.

This selection follows closely the cut-based, missing-energy channel of the Higgs boson search [2]. However, because the masses of the final state particles are known, the mass information can be used effectively to reject much of the background. As for the other channels, an elliptical mass cut with a cut on the “radius”

$$r^2 = \left( \frac{m_{\text{rec}} - m_Z}{\sigma_{m_{\text{rec}}}} \right)^2 + \left( \frac{M - m_Z}{\sigma_M} \right)^2$$

is used, where  $\sigma_{m_{\text{rec}}} = 3.1 \text{ GeV}/c^2$  and  $\sigma_M = 8.5 \text{ GeV}/c^2$  are the approximate resolutions. The quantity  $m_{\text{rec}}$  is the invariant mass of the two jets with the missing mass constrained to  $m_Z$ . Figure 3 shows the reconstructed mass distribution from the  $q\bar{q}\nu\bar{\nu}$  analysis with the elliptical mass cut removed.

The performance is shown in Table I. The numbers in this table have been corrected for unsimulated accelerator backgrounds which increase the energy near the beamline. The size of the full correction has been used as an estimate of the systematic uncertainty. Similarly, the jet kinematics have been corrected to make them better correspond to those observed in the data. Again the full size of this correction is used as the systematic uncertainty. The systematic uncertainties also include uncertainties from the Z branching fractions, background production cross sections, and the limited statistics of the MC samples. As the uncertainty on the luminosity is correlated between all channels it is included only in the combination. Adding these uncertainties in quadrature gives total relative uncertainties of 2.2% and 5.3% on the signal and background, respectively.

#### E. $q\bar{q}\nu\bar{\nu}$ (NN Analysis)

A neural network has been constructed using all 12 variables from one of the two neural networks used in the  $h\nu\bar{\nu}$  analysis [2] including the reconstructed  $q\bar{q}$  invariant mass. Two of the twelve variables come from the neural network b-tagger outputs for the two quark jets. Even though  $ZZ \rightarrow b\bar{b}\nu\bar{\nu}$  is only a fraction of the total  $Z\nu\bar{\nu}$  samples, the b-tagging is useful in improving the selection in that subsample without affecting the performance on other subsamples.

Table I summarizes the performance of this selection.

Systematic uncertainties are estimated from effects of jet energy smearing, unsimulated accelerator backgrounds, b-tagging uncertainties, and limited Monte Carlo statistics. The relative uncertainty on the ZZ signal efficiency is 5%, and the relative uncertainty on the expected background 10% (6.5 events).

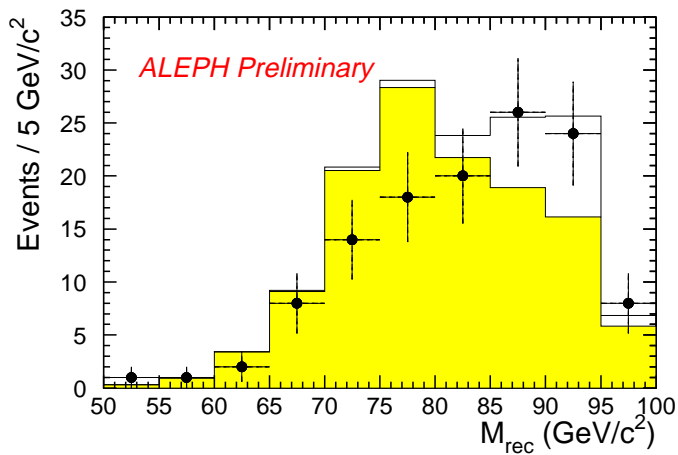


FIG. 3. The distribution of masses for the  $q\bar{q}\nu\bar{\nu}$  channel. The expectation from the Standard Model is shown for comparison. The grey region is the contribution from the backgrounds and the white region that from the  $\mathcal{NC}2$  signal.

In much the same way as for the  $q\bar{q}q\bar{q}$  case, the neural network output distribution is split into ten pieces. When these pieces are combined, the expected uncertainty on the cross section is 31%, compared to an expected uncertainty of 33% when the shape of the distribution is not considered.

### F. $\ell^+\ell^-\nu\bar{\nu}$ Channel

Despite its small contribution to the total  $ZZ$  cross section, a dedicated selection has been devised for the  $\ell^+\ell^-\nu\bar{\nu}$  channel.

The preselection requires events with exactly two identified electrons or muons and no other reconstructed charged particles. These leptons must have the same flavor and opposite charge. The fraction of the total energy deposited in the central part of the detector,  $f_{30^\circ}$ , must be approximately half the total center-of-mass energy,  $0.4 < f_{30^\circ} < 0.6$ . The acoplanarity of the two leptons must be less than  $178^\circ$ .

As for the  $q\bar{q}\nu\bar{\nu}$  channel, cuts on other kinematic quantities further suppress the background. The invariant mass of the leptons and of the missing mass are required to be within an ellipse of  $r < 1.7$ , defined as above, with  $\sigma_M = 3.3 \text{ GeV}/c^2$  and  $\sigma_{m_{\ell\ell}} = 2.5 \text{ GeV}/c^2$ . The missing momentum must point away from the beamline,  $\theta_{\cancel{p}} > 6.7^\circ$ , and the total energy not associated with the leptons must be less than 5.6 GeV.

The performance of this selection is summarized in Table I.

### G. $\tau\tau q\bar{q}$ Neural Network Selection

This selection is based on the  $hA \rightarrow \tau\tau b\bar{b}$  event selection [2]. A new neural network, trained specifically for  $ZZ$  selection, has the same structure as the  $hA$  neural network, but uses the reconstructed mass instead of the b-tagging output as one of the five input variables.

Table I summarizes the performance of this selection.

Systematic uncertainties on the signal efficiency are estimated to be 2.0% due to jet angle uncertainties and 2.2% due to limited Monte Carlo statistics, leading to a total relative uncertainty on the signal efficiency of 3.0%. The relative uncertainty on the expected number of background events is 10.8% (0.16 events), the major part of which is from limited Monte Carlo statistics.

TABLE I. Summary of the efficiencies, expected backgrounds, numbers of observed events, and the measured cross sections for each channel. (The symbol  $\ell$  denotes only electrons and muons.)

	“Cut”	“NN”	$\epsilon$ (%)	$N_{\text{bkg}}$	$N_{ZZ}^{\text{SM}}$	$N_{\text{obs}}$	$\sigma_{\mathcal{N}C2}$ (pb)
$\ell\ell XX$	✓	✓	$76.5 \pm 1.5$	$1.1 \pm 0.3$	8.7	11	$0.72 \pm_{0.22}^{0.27}$
$q\bar{q}q\bar{q}$ (b)	✓		$39.4 \pm 0.5$	$3.8 \pm 0.4$	8.1	13	$0.71 \pm 0.28$
$q\bar{q}q\bar{q}$ (non-b)	✓		$47.0 \pm 0.4$	$59.9 \pm 1.4$	15.7	67	$0.29 \pm 0.32$
$q\bar{q}q\bar{q}$		✓	$31.5 \pm 1.0$	$19.7 \pm 2.7$	16.8	31	$0.56 \pm 0.20$
$q\bar{q}\nu\bar{\nu}$	✓		$47.1 \pm 0.3$	$13.8 \pm 0.6$	14.4	29	$0.66 \pm 0.23$
$q\bar{q}\nu\bar{\nu}$		✓	$80.1 \pm 4.0$	$65.1 \pm 6.5$	24.5	88	$0.67 \pm 0.20$
$\ell\ell\nu\bar{\nu}$	✓	✓	$44.6 \pm 1.5$	$1.4 \pm 0.2$	1.3	1	$-0.20 \pm_{0.30}^{0.66}$
$\tau\tau q\bar{q}$		✓	$42.2 \pm 1.3$	$1.48 \pm 0.16$	2.2	3	$0.45 \pm_{0.41}^{0.62}$

### III. COMBINATION OF CHANNELS

Table I summarizes the efficiencies, numbers of events observed, etc. for all of the channels. A maximum likelihood fit determines the  $\mathcal{N}C2$  cross section for  $e^+e^- \rightarrow ZZ$  by combining information from all of the channels. For the neural-network based analysis, a binned likelihood is used for the  $q\bar{q}q\bar{q}$  and  $q\bar{q}\nu\bar{\nu}$  channels where the shape of the neural-network distribution is used; for the other channels and for the cut-based analysis, only the total numbers of events are used in the likelihood.

The expected relative statistical uncertainties on the 188.6 GeV cross section measurements of 20.0% and 18.6% for the cut-based and neural-network based analyses, respectively was determined with toy Monte Carlo experiments. The systematic uncertainty was determined by adding a Gaussian smearing to the efficiencies and background estimates to the toy Monte Carlo experiments.

Common contributions to the total systematic uncertainty of the measurement are the luminosity (1.5%) and the (very small) overlap between the various channels (0.5%). The total relative systematic uncertainties are 5.5% and 9.7% for the cut-based and neural-network based analyses, respectively.

The measured cross sections at  $\sqrt{s} = 188.6$  GeV are

$$\sigma_{\mathcal{N}C2} = 0.63 \pm 0.12 \text{ (stat.)} \pm 0.05 \text{ (syst.) pb and}$$

$$\sigma_{\mathcal{N}C2} = 0.62 \pm 0.12 \text{ (stat.)} \pm 0.06 \text{ (syst.) pb.}$$

for the cut-based and neural-network based analyses, respectively, compared to the Standard Model expectation of 0.63 pb. Table I shows the cross section for each channel individually.

This cut-based analysis has also been applied to the 1997 data sample. The measured cross section is

$$\sigma_{\mathcal{N}C2} = 0.22 \pm_{0.22}^{0.18} \text{ (stat.)} \pm 0.04 \text{ (syst.) pb.}$$

at a center-of-mass energy of  $\sqrt{s} = 182.7$  GeV compared to the Standard Model expectation of 0.25 pb.

### IV. CONCLUSIONS

Two analyses have measured the  $ZZ \mathcal{N}C2$  cross section using the recent data taken in 1998. Both analyses agree with each other and with the Standard Model value of 0.63 pb. The  $ZZ$  production cross section is measured to be

$$\sigma_{\mathcal{N}C2} = 0.63 \pm 0.12 \text{ (stat.)} \pm 0.06 \text{ (syst.) pb.}$$

at  $\sqrt{s} = 188.6$  GeV.

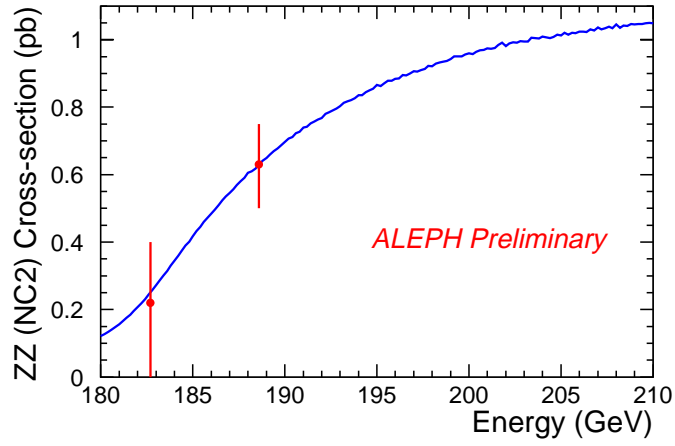


FIG. 4. The measured  $\mathcal{NC}2$  cross sections compared to the expected Standard Model cross section.

Additionally, the cut analysis has been applied to the 1997 data sample yielding a measurement of

$$\sigma_{\mathcal{NC}2} = 0.22 \pm_{0.22}^{0.18} \text{ (stat.)} \pm 0.04 \text{ (syst.) pb.}$$

at a center-of-mass energy of  $\sqrt{s} = 182.7$  GeV.

Figure 4 compares the measured values with the Standard Model expectation [1].

- [1] T. Sjöstrand, *The PYTHIA 5.7 and JETSET 7.4 Manual*, LU-TP.95/20 and CERN-TH.7112/93.
- [2] ALEPH Collaboration, “Search for the Neutral Higgs Bosons of the Standard Model and the MSSM in  $e^+e^-$  Collisions at  $\sqrt{s} = 188.6$  GeV”, ALEPH 99-007 (CONF 99-003) available from <http://alephwww.cern.ch/>; ALEPH Collaboration, *Phys. Lett.* **B447**, 336 (1999); ALEPH Collaboration, *Phys. Lett.* **B440**, 419 (1998) with erratum *Phys. Lett.* **B447**, 355 (1999).
- [3] ALEPH Collaboration, *Measurement of the W Mass by direct Reconstruction in  $e^+e^-$  Collisions at 172 GeV*, *Phys. Lett.* **B422**, 384 (1998).